Available online at www.sciencedirect.com

ScienceDirect

journal homepage: www.elsevier.com/locate/he

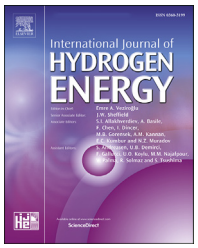

Microvoids in electrochemically hydrogenated titanium-based alloys

Eli Brosh [a,b,1], *Nissim U. Navi* [b], *Brian A. Rosen* [a], *Noam Eliaz* [a,*]

[a] *Department of Materials Science and Engineering, Tel-Aviv University, Ramat Aviv, Tel Aviv, 6997801, Israel*
[b] *Nuclear Research Center Negev (NRCN), P.O. Box 9001, Beer Sheva 84190, Israel*

HIGHLIGHTS

- Microvoids are observed in wrought Ti–6Al–4V after electrochemical hydrogenation.
- Such voids do not form in wrought, single-phase, CP-Ti.
- Such voids are abnormal in hydride-forming metals with exothermic heat of solution.
- Shrinkage due to hydride precipitation is suggested as leading to void formation.
- Multiphase and fast diffusion paths into the bulk alloy promote void formation.

ARTICLE INFO

Article history:
Received 10 March 2021
Received in revised form
25 May 2021
Accepted 26 May 2021
Available online 19 June 2021

Keywords:
Hydrogen embrittlement (HE)
Bubble
Microvoid
Additive manufacturing (AM)
Ti–6Al–4V alloy

ABSTRACT

In a recent study, it was observed that electrochemical charging with hydrogen produces microvoids both in wrought and in additively manufactured, electron beam melted (EBM) Ti–6Al–4V alloys. This result is surprising since titanium forms stable hydrides and has an exothermic heat of hydrogen solution. By comparison, hydrogen bubble formation is typically observed only in metals and alloys with an endothermic heat of hydrogen solution that do not form hydrides. Here, we evaluate possible mechanisms for the formation of microvoids and bubbles in Ti-based alloys. Additional experimental work confirms that voids do not form in electrochemically hydrogenated, single-phase, pure wrought Ti, whereas they do form in the wrought Ti–6Al–4V alloy hydrogenated under the same conditions. In commercially pure Ti (CP–Ti), hydride is formed from the surface inward, and the surface is brittle and heavily cracked and disintegrated. By contrast, in the two-phase alloy, hydrides are formed also deeper in the bulk, and microvoids are evident both adjacent to the surface and along interphase boundaries. Alongside the forming hydride, the surface integrity is maintained, although some cracks are formed due to microvoid coalescence. While the incorporation of hydrogen into the alloy causes a large increase in its volume, we note that the precipitation of hydride from a supersaturated solution causes a net contraction. We suggest that the mechanism that best reflects the experimental evidence of microvoids formation is a manifestation of the contraction that results from hydride precipitation from a hydrogen-supersaturated alloy.

* *Corresponding author.*
E-mail address: neliaz@tau.ac.il (N. Eliaz).
[1] Work done during sabbatical leave at Tel-Aviv University.

https://doi.org/10.1016/j.ijhydene.2021.05.187

Introduction

One of the most common mechanisms of hydrogen embrittlement of metals is high-pressure bubble formation, according to which bubbles filled with molecular hydrogen can form in metals with an endothermic enthalpy of hydrogen solution under conditions of high hydrogen fugacity [1–4]. When the pressure developed inside these bubbles is sufficiently high, microcracks might initiate and emanate from them, even in the absence of applied load [5–7]. In the case of metals with an exothermic enthalpy of hydrogen solution, the hydrides of which are either stable or can be stabilized by an applied stress (e.g. Ti, Zr, or Nb), the hydride formation mechanism was suggested to describe their embrittlement [8,9].

Recently, Navi et al. [10] observed by light microscopy and scanning electron microscopy (SEM) microvoids either adjacent to the surface or along $\alpha/\alpha_H//\beta/\beta_H$ interphase boundaries, both in wrought and in electron beam melted (EBM) Ti–6Al–4V alloys, after electrochemical hydrogenation. The amount of α/β interphase boundaries, hydride and microvoid formation, as well as cracking along interphase boundaries were more significant in the EBM alloy than in the wrought alloy. The fact that voids appeared also in the extra-low interstitial (ELI) wrought alloy suggests that they are neither filled by a gas that is a product of a hydrogen-impurity reaction, nor the product of gas entrapment during the additive manufacturing (AM) process. Recent research revealed that oxygen plays an important role in phase transformation of titanium hydrides [11]. Also, oxygen impurity-assisted mechanism of hydrogen bubble nucleation in tungsten, according to which stable vacancy-oxygen-hydrogen complexes form, was proposed [12]. Interestingly, voids as those reported in Ref. [10] were not reported by others for either wrought [13] or EBM [14] Ti–6Al–4V alloys, following electrochemical hydrogenation in a similar electrolyte. However, we do identify some microvoids in the vicinity of cracks in Fig. 2 in Ref. [13] (SEM image of wrought Ti–6Al–4V after electrochemical hydrogenation for 69 h at $j = 50$ mA/cm^2 in a 1:2 H_3PO_4:glycerine electrolyte). We cannot tell whether the formation of these microvoids was overlooked at that time, or if they existed also in the non-hydrogenated alloy.

The formation of microvoids in titanium due to hydrogenation is an unexpected result since the partial enthalpy of hydrogen solution in Ti is negative, and stable titanium hydrides are formed [15]. While void nucleation was reported for coarse-grained commercially pure titanium (CP–Ti) under equibiaxial tension due to hydride fracture [16], and hydrogen trapping in vacancies [17,18] may be the first stage in hydrogen bubble formation, we could not find conclusive experimental evidence for the presence of microvoids or bubbles in hydrogenated Ti or Ti-based alloys.

Vanadium is another well-studied hydride-forming metal with exothermic enthalpy of hydrogen solution. Since this enthalpy is slightly less negative than that of Ti, some possible mechanisms of hydrogen bubble formation would predict more bubbles in V than in Ti. Yet, even in the case of V, no observations such as in Ref. [10] have been reported. On the other hand, hydrogen ion irradiation at room temperature (RT) was reported [19] to yield small dislocation loops and cavities, which led to bubble coalescence only during annealing at 500 °C. Hultgren and Scott [20] reported blister formation in both V and Nb as a result of proton bombardment at RT, despite the temperatures being lower than the top miscibility gap temperatures. Below these temperatures, vanadium and niobium hydrides are stable relative to gaseous hydrogen even at low hydrogen partial pressures. A model for this radiation blistering was not provided. Recently, first principles calculations of the hydrogen-hydrogen and vacancy cluster-hydrogen interactions showed that hydrogen self-clusters are unlikely to occur in V and cannot act as initiation sites for hydrogen bubble growth [21].

The objective of this work is to discuss possible mechanisms for hydrogen-induced formation of microvoids and bubbles in Ti-based alloys and suggest the one that best reflects our experimental data on EBM and wrought Ti–6Al–4V alloys. Hydrogenation of CP-Ti was performed in order to elucidate whether the presence of two or more phases in the microstructure is vital for void formation. Some complementary hydrogenation experiments were performed also on wrought Ti–6Al–4V alloy in order to verify reproducibility and that void formation was not affected by a specific hydrogenation cell setup and the formation of black residues of the type reported in Ref. [10].

Materials and methods

Comparison was made between wrought CP-Ti Grade 2 (ASTM F67–00, max 0.25 wt% O, 5 mm thick plate, supplied by Barmil Ltd.) and wrought Ti–6Al–4V Grade 23 (ELI, ASTM F136) rod (25.4 mm in diameter, produced by Dynamet, Inc., Washington, PA). Based on the material test report of the manufacturer (ATI, Washington, PA), the CP-Ti contained 0.16 wt% O, 0.13 wt % Fe, 0.011 wt% C, 0.007 wt% N, and the balance – Ti. Both materials were cut by electric discharge machining (EDM), mechanically ground and polished on both sides down to 1 μm abrasive and sample thickness of 0.3 mm. Both sample types were hydrogenated electrochemically in a two-electrode cell at RT for 4 days. The electrolyte was H_3PO_4:glycerin (1:2 vol) with Ar purging, and the charging current density was $j = -25$ mA/cm^2. The cell geometry was modified compared to Ref. [10], the circumferential anode being pure Pt foil instead of $Pd_{90}Pt_{10}$ (wt%).

The microstructure of samples before and after hydrogenation was characterized on metallographic cross-sections using both a light microscope (AXIS, Zeiss, Oberkochen, Germany) and SEMs (Quanta 200 FEG, FEI, The Netherlands & Gemini 300, Zeiss, Germany). X-ray diffraction (XRD) at RT was used for phase identification and phase content analysis of the sample's surface. XRD measurements were performed using a D8 ADVANCE diffractometer with a Bragg-Brentano geometry (Bruker AXS, Madison, WI, USA) and Cu-Kα radiation source ($\lambda = 1.5418$ Å). The lattice parameters were fitted by Rietveld refinement, using TOPAS software, ver. 5 (Bruker AXS, Madison, WI, USA), fitting for the displacement error, lattice parameters, microstrain and phase composition. NIST Si 640e and LaB_6 660c standard reference materials were used to calibrate for peak position and peak shape, respectively. Peaks were fitted using a TCHZ function type, where U,W,V

and the asymmetry parameters were measured using LaB_6 660c and fixed to account for instrumental contributions to peak shape.

Experimental results

The XRD patterns of CP-Ti before and after hydrogenation are shown in Fig. 1 a. The reflections of the non-hydrogenated α(hcp) Ti are indexed according to the International Center for Diffraction Data (ICDD) file no. 00-044-1294. The space group of this phase is $P6_3/mmc$ (194). The strongest reflection of the non-hydrogenated CP-Ti in Fig. 1a is (002), and not (101) as in the ICDD file. This indicates preferred orientation (texture) of the Ti sheet, possibly due to well-defined, platy habits [22]. The small peak at $2\theta = 36.7°$ appears to belong to a titanium oxide such as anatase, but one could not determine it unambiguously based on one reflection only. The microstrain in the non-hydrogenated CP-Ti α(hcp) was $6.7 \pm 1.0 \times 10^{-4}$.

After hydrogenation, the peaks of α-Ti disappear, and only a hydride phase is evident, which is most likely a cubic δ-TiH_2 (indexed according to ICDD file no. 01-071-4960). This hydride has space group $Fm\bar{3}m(225)$. Due to the peak at ca. 88.5°, which is unique to the cubic phase, the tetragonal TiH_2 phase (ICDD No. 00-009-0371) is ruled out. The strongest reflection of the hydrogenated CP-Ti matches the strongest reflection in the ICDD file. The small peaks at ~36.5° and ~39° appear to belong to a cubic sub-stoichiometric titanium hydride similar to $TiH_{1.91}$ (ICDD No. 04-002-5206). However, owing to the small amount of this secondary hydride, and the limited number of

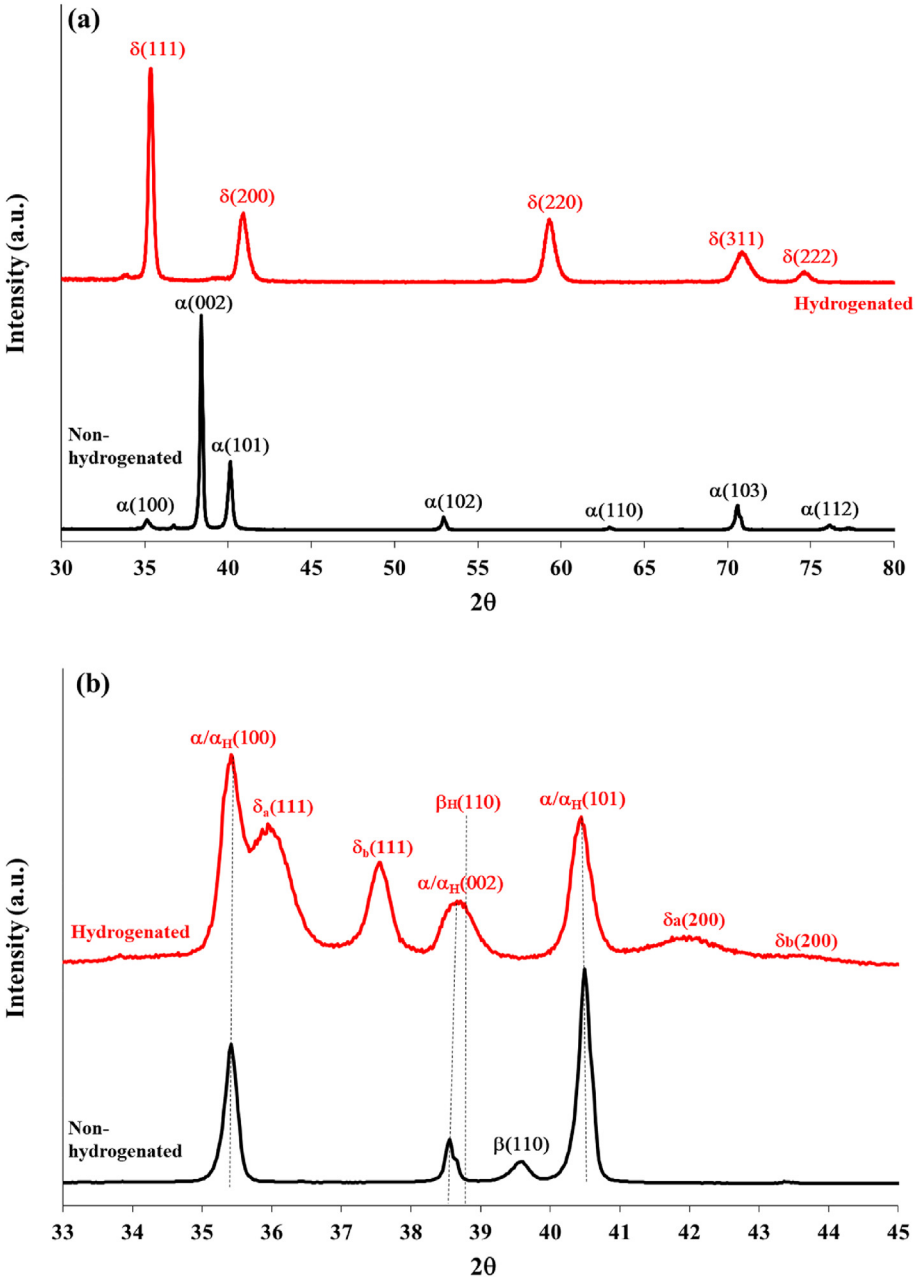

Fig. 1 – XRD patterns of non-hydrogenated and 4-day hydrogenated wrought CP-Ti (a) and wrought Ti–6Al–4V alloy (b).

peaks, quantitative analysis is less reliable here and they are not part of the fit. The microstrain in the hydrogenated CP-Ti (hydride phase) was $20.0 \pm 5.0 \times 10^{-4}$. As expected, hydrogenation and the formation of hydride resulted in an increase in the microstrain in the material.

The XRD patterns of the wrought Ti–6Al–4V alloy, before and after hydrogenation, are shown in Fig. 1b. Despite the replacement of the $Pd_{90}Pt_{10}$ anode by a pure Pt anode, and consequently the elimination of black residues as those observed in Ref. [10], the results reproduce well those in Ref. [10], namely: the hydrogenated alloy contains α/α_H (cannot be distinguished from the XRD pattern), along with a β_H solid solution and two hydrides with a fcc structure and space group $Fm\bar{3}m$ (225) – δ-TiH_2-like (δ_a) and δ-TiH_x-like (δ_b). As evident from Table 1, the lattice parameter of β_H is larger than that of β due to the high solubility of hydrogen in the β phase. In contrast, the lattice parameters of α/α_H in the hydrogenated alloy are more similar to those in the non-hydrogenated alloy due to the low solubility of hydrogen in the α phase at RT [10]. It is also evident from Table 1 that the hydrogenated alloy contains ca. 50% solid solutions and 50% hydrides in vicinity of its surface. The β_H content in the hydrogenated alloy is similar to that of β in the non-hydrogenated alloy (within the Rietveld refinement uncertainty), as reported in Ref. [10]. As reported in Ref. [10], the microstrain in the non-hydrogenated wrought alloy was $3.0 \pm 1.0 \times 10^{-4}$ in the α-phase and zero in the β-phase. After four-day hydrogenation, the microstrains in the α/α_H-phase and β_H-phase increased to $23.0 \pm 1.0 \times 10^{-4}$ and $46.0 \pm 4.0 \times 10^{-4}$, respectively. The microstrains in δ_a-hydride and δ_b-hydride were $63.0 \pm 2.0 \times 10^{-4}$ and $18.0 \pm 2.0 \times 10^{-4}$, respectively.

In Fig. 2, a comparison is made between the cross-sections of the 4-day hydrogenated wrought CP-Ti (a,b) and the wrought Ti–6Al–4V alloy (c,d) as observed in the SEM. The defects in the vicinity of the surfaces for both samples are quite different. In the Ti–6Al–4V alloy, the structural integrity is maintained, but microvoids are evident both adjacent to the surface and in the bulk alloy. It was reported in Ref. [10] that these voids preferentially nucleate and grow at $\alpha/\alpha_H/\beta_H$ interphase boundaries. Some void coalescence is evident around cracks, possibly indicating the mechanism by which these cracks were formed. By contrast, the zone beneath the surface of hydrogenated CP-Ti is clearly brittle and heavily cracked; yet, no microvoids are evident in this case. Since such severe damage in hydrogenated CP-Ti has rarely been reported, and the sample was neither defected before hydrogenation nor exposed to an applied load, it can be concluded that the H_3PO_4:glycerin (1:2 vol) electrolyte [10,23,24] is very efficient in promoting atomic hydrogen adsorption at the metal surface. This is followed by hydrogen absorption into the metal owing to the high viscosity of the glycerin, even without containing surface poisons. Hydrogen effects on CP-Ti are clearly more pronounced than on Ti–6Al–4V, as reflected by higher susceptibility to hydrogen embrittlement and hydrogen-induced cracking (as evident from the SEM images) and significantly higher degradation of phase stability (as evident from X-ray diffractograms). These effects can be explained by the significantly lower solubility of hydrogen in the α-phase, which is the only phase in the microstructure of CP-Ti, and by the transformation of α in Ti–6Al–4V into hydrides such as those reported in Ref. [10] and identified again herein.

Table 1 – The lattice parameters and the content of the phases in non-hydrogenated and hydrogenated CP-Ti and Ti–6Al–4V based on Rietveld refinement.

	CP-Ti		Ti–6Al–4V alloy		Phase content
	a, *b* (Å)	*c* (Å)	*a*, *b* (Å)	*c* (Å)	(wt.%, ± ca. 1%)
Non-hydrogenated					
α	2.9556	4.6894	2.9203	4.6578	93.13 [10]
β			3.2171		6.87 [10]
Hydrogenated					
α/α_H			2.9172	4.6874	43.38
β_H			3.2851		8.44
δ_a			4.3040		45.98
δ_b			4.1410		2.20
δ	4.4146				

Mechanisms of microvoids formation

In the context of the following discussion, the difference between voids and bubbles in the metal should be noted. Bubbles are spherical cavities filled with gas whereas voids are empty spaces (vacuum), e.g. clusters of vacancies in the crystal lattice. The rounded shape of the microvoids observed in the hydrogenated Ti–6Al–4V alloy suggests that they may have originated as gas bubbles. It is concluded that such bubbles must be filled with hydrogen gas since no other gas was present in the system.

Condon and Schober [1] pointed out that in order to precipitate in a bubble, the chemical potential of dissolved hydrogen must be at least equal to that of the gas in the bubble. For the bubble to grow, the pressure inside it must be at least as large as required for plastic deformation of the matrix by "dislocation punching" [1,25], which may be as high as a few GPa [1]. Hence, the chemical potential of the gas in the bubble must be higher than that at atmospheric pressure.

In Fig. 3, the chemical potential of dissolved hydrogen is calculated with two up-to-date thermodynamic models [26,27]. The use of such thermodynamic models should be more accurate than the Henrian solution model implied by equation (10) in Hou et al. [25]. A lower limit for the minimal hydrogen concentration for bubble precipitation may be estimated by observing the point where the calculated curves equal zero. That is, the concentration at which the chemical potential of dissolved hydrogen equals that of hydrogen gas at standard conditions. It can be seen in Fig. 3 that the concentration of hydrogen required for precipitation from α-Ti (hcp) is lower than that required for precipitation from β-Ti (bcc). It is thus concluded that if hydrogen indeed forms bubbles, the single α-phase CP-Ti should be more prone to this phenomenon than the dual-phase Ti–6Al–4V alloy. However, this conclusion is in contrary to the experimental results shown above.

Also in Fig. 3, it is shown that the concentration of dissolved hydrogen required for precipitation is relatively large, at least 33 at%. This value is significantly higher than the

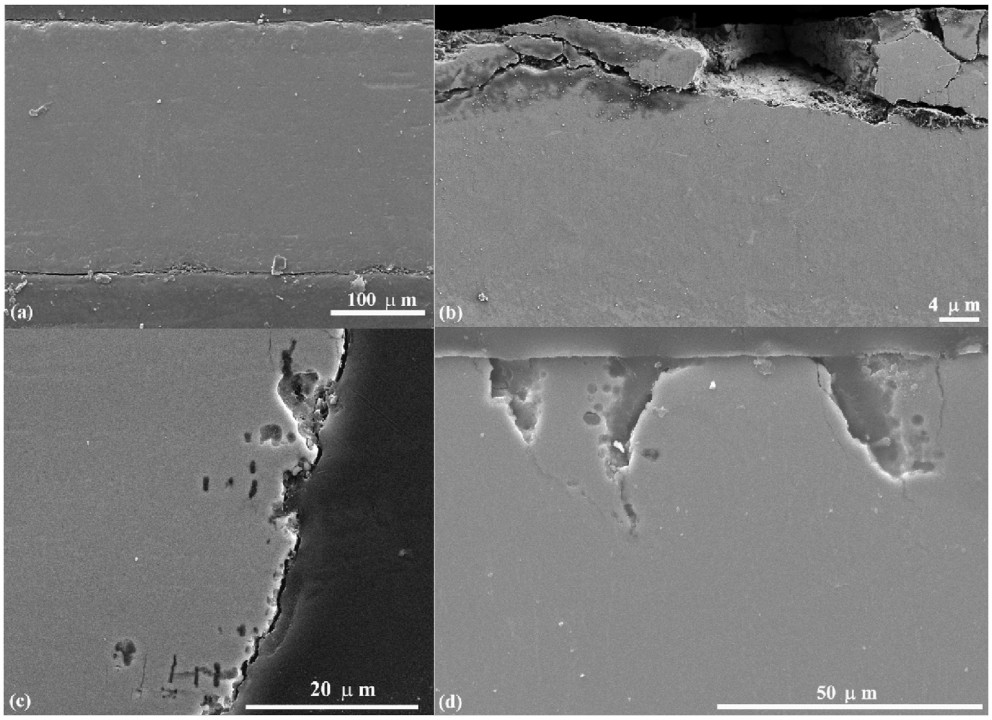

Fig. 2 – SEM images of 4-day hydrogenated wrought CP-Ti (a,b) and wrought Ti–6Al–4V alloy (c,d).

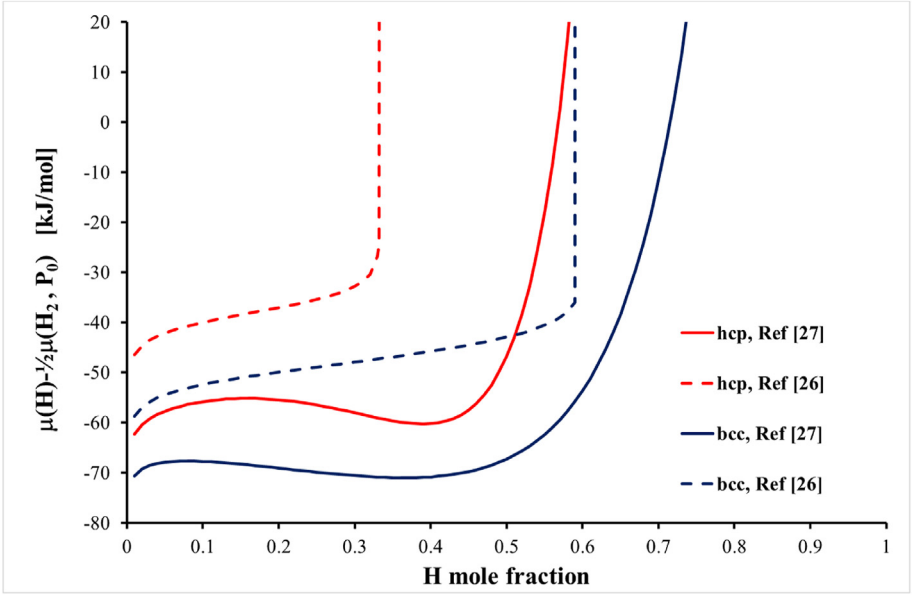

Fig. 3 – Chemical potential of interstitial hydrogen in Ti at T = 298.15 K relative to gas at atmospheric pressure. The calculation was performed without allowing miscibility gaps, but this has no influence on the conclusions drawn herein.

1–15 at% concentration that would cause the formation of hydrides in the Ti–H system [15] in general, and in Ti–6Al–4V specifically [28]. Hence, it seems that if the high hydrogen concentration of at least 33 at% is attained locally, a hydride will form rather than bubbles. Indeed, hydrides are formed in Ti–6Al–4V, also at the same distance from the surface as the observed voids. Therefore, based on Fig. 3, the interpretation of voids in hydrogenated Ti–6Al–4V as originating from bubbles that precipitated because of hydrogen supersaturation may be ruled out.

An alternative view of the situation is based on the observation of volume changes occurring during hydride precipitation. When hydrogen is incorporated into the alloy, the volume of the alloy expands. This is evident from the fact that the volume per mole of TiH_x is much larger than the volume per mole of metallic Ti either in the α or in the β phase.

However, below we consider the volume change that occurs when hydride precipitates from a supersaturated solution, which is a different process, distinct from hydrogen incorporation in the alloy.

The reaction of dissolved hydrogen, H_{int}, with metal to form hydride:

$$xH_{int} + M \rightarrow MH_x \quad (1)$$

is accompanied by the overall volume change per mole:

$$\Delta V = V_{MHx} - V_M - xV_H \quad (2)$$

where x is the ratio H/M in the hydride, V_{MHx} is the molar volume of the hydride, V_M is the molar volume of the reacting metal, and V_H is the partial molar volume of dissolved hydrogen. The relative volume change is computed as:

$$\frac{\Delta V}{V_M + xV_H} \quad (3)$$

The molar volumes of the δ-hydrides of titanium, as well as other parameters in Eq. (2) are given in Table 2. In Fig. 4, the calculated relative volume change (3) is shown. It is evident that as a result of hydride formation, the volume of the alloy decreases. Thus, for a given (local) composition, hydride formation leads to shrinkage. As shown by the above calculations, the precipitation of hydride from a metal-hydrogen solution causes an overall decrease in volume. This requires some explanation.

Incorporation of hydrogen in the alloy, either dissolved in the metallic phases or as a hydride, causes an increase in the alloy's volume. Moreover, the volume of the precipitated hydride is larger (per mole of metal) than the volume of the metal. This causes a misfit. The hydride is in a state of compression while the surrounding metal matrix is under tension. The transition of hydrogen atoms from the solid solution matrix to the hydride causes an increase in the volume of the hydride and increases the misfit stress. Concurrently, the volume of the matrix around the hydride precipitate decreases because hydrogen is leaving the matrix, going into the hydride phase. The partial molar volume of hydrogen in the matrix is larger than the volume occupied by a mole of hydrogen atoms in the hydride [29], hence this process results in an overall decrease in volume of the whole system. We suggest that under special conditions, such as in the present work, this overall shrinkage may result in formation of microvoids in the matrix. Such microvoids are likely to form in vicinity of the precipitating hydride, but probably not at the hydride/matrix interface.

As noted by Östberg et al. [30], this shrinkage effect has nothing to do with the misfit stresses around the precipitate, which are quite large. We note that the shrinkage calculated for the precipitation process is not in contradiction with the overall increase in the alloy volume as a result of the

Table 2 – Molar volume parameters for Eq. (2), applied to titanium and zirconium.

	Parameter	[cm^3/mol]	Source
Ti	$V^{\delta}_{TiH_x}$	$11.3465 \cdot (1 + 0.02663 \cdot x)^3$	Calculated from lattice parameter data for $1.56 < x < 1.8$ [35]
	V^{α}_{Ti}	10.635	[36]
	V^{β}_{H}	1.6[a]	[37–39]
Zr	$V^{\delta}_{ZrH_x}$	16.44	Calculated from lattice parameter data for $1.5 < x < 1.67$ [40]
	V^{α}_{Zr}	14	[41]
	V^{α}_{H}	1.7 (average)	[42]

[a] The chosen value is equal to that in Ref. [38]. It is larger than that in Ref. [37], but smaller than the lower limit of the range in Ref. [39].

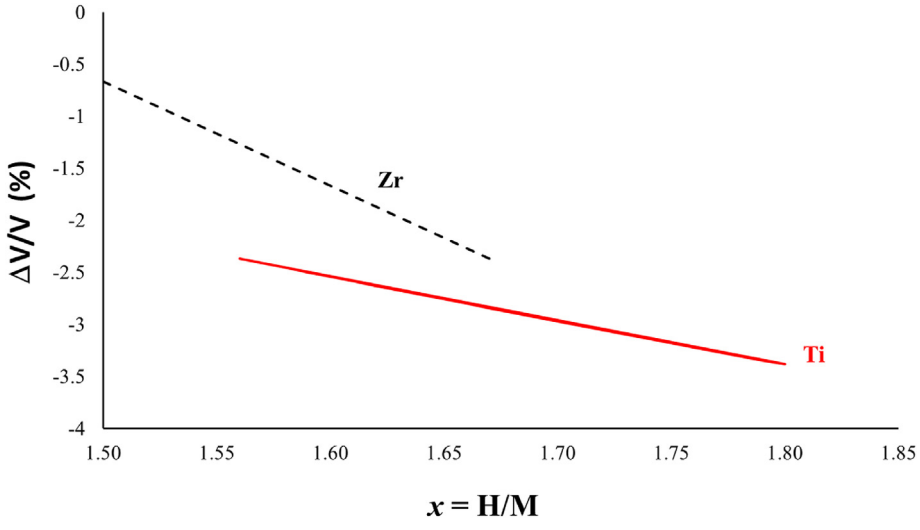

Fig. 4 – Relative volume change due to formation of δ-hydride from titanium and zirconium.

incorporation of hydrogen. Shrinkage may occur only when the precipitation of hydride is delayed, i.e., after the hydrogen is already dissolved in the alloy. While we could not find direct experimental verification of this shrinkage in titanium alloys, it is evident from dilatometric measurements in Zr-alloys. For example, Singh et al. [31] found by dilatometric measurements that dissolution of hydrides in Zr alloys upon heating caused an increase in sample volume while precipitation of hydrides upon cooling the alloy caused shrinkage. Östberg et al. [30] used dilatometry to measure volume changes accompanying precipitation of hydrides in Zr and observed shrinkage. Experimental observations similar to those of Singh et al. were reported by other researchers as well [32–34]. The results of a simple calculation presented in Fig. 4 imply that the same effect should be even stronger in Ti alloys.

It is proposed that under certain conditions this shrinkage may lead to void formation. Two distinct situations are depicted in Fig. 5. In Fig. 5a, the electrochemical hydrogenation of a single-phase metal such as CP-Ti is shown. Hydrogenation takes place within a near-surface layer. The layer is cracked because of the misfit stresses and the brittleness of the formed hydride. When shrinkage occurs, it is compensated by the overall swelling as a result of hydrogen intake. Also, being close to the surface, shrinkage is manifested simply by its effect on the outer specimen dimensions. Fig. 5b shows the electrochemical hydrogenation of a two-phase alloy, e.g. Ti–6Al–4V. Hydrogen diffusion into the alloy occurs predominantly through one of the phases. This is in fact the situation in the Ti–6Al–4V alloy where the diffusion of hydrogen is likely to take place in the β phase, because the diffusion coefficient in this phase is significantly higher, as is the solubility of hydrogen [13,43–45]. First, certain places in the material become saturated, and only then hydride precipitation occurs, i.e., hydride precipitation is delayed. Additionally, hydride formation takes place not only in the thin near-surface layer but also further away from the surface, as observed experimentally in Ref. [10]. The delay in hydride formation could thus be related to the hydrogenation at low (room) temperature where only fast-diffusing paths through the β phase operate, and so the hydride precipitation may occur far from the surface.

The proposed mechanism is in line with the experimental observations reported both in Refs. [10,46] and in the present study: (1) the high density of α/β interphase boundaries favor local hydride nucleation and growth; (2) δ_a and δ_b hydrides are transformed from the primary α-phase in Ti–6Al–4V; (3) electrochemical hydrogenation results in formation of microvoids in both wrought and EBM Ti–6Al–4V alloys, either adjacent to the surface or along $\alpha/\alpha_H//\beta/\beta_H$ interphase boundaries in the bulk metal; (4) hydrogen penetrates through the whole bulk sample and hydride formation occurs in the bulk metal, not just within the surface layer, based on time-of-flight secondary ion mass spectrometry (ToF-SIMS) analysis; (5) the microstructure of EBM Ti–6Al–4V alloy with more α/β interphases promotes the α/α_H-to-δ_a phase transformation and makes the EBM alloy more prone to hydrogen-induced cracking compared to wrought Ti–6Al–4V.

In Ti–6Al–4V, hydride precipitation occurs predominantly at the α/β interphase boundaries. Therefore, in the calculation of shrinkage it was assumed that in the hydride formation reaction, the β phase was the source of hydrogen atoms while the α phase was the source of titanium atoms. This may be regarded as a delayed hydride precipitation; hydrogen first dissolves in the β phase, and the precipitation occurs later by reaction with the titanium in the α phase. When this precipitation occurs in the bulk of the material, shrinkage cannot be accommodated by a change in the outer dimensions of the sample, hence it takes place locally, leaving voids that contain some hydrogen. The pressure of hydrogen in the so-developed bubbles may be lower than atmospheric; hence, the threshold concentration for its precipitation as molecular species is lower than it would be if the pressure were atmospheric or higher. The proposed mechanism for the formation of hydrogen-filled microvoids is not competing with hydride formation, but rather results from the hydride precipitation. Hence, it should result in bubbles appearing in the immediate vicinity of the hydride precipitates. One consequence of the proposed mechanism is that the formation of microvoids is expected to depend on the area of α/β interfaces as well as on the β-content in the duplex alloy. This is in line with the experimental observation of more microvoids in the EBM alloy than in the wrought alloy. It is also anticipated that due to the higher solubility of hydrogen in Ti-based alloys with higher β-contents, the driving force for hydride precipitation will be lower, and consequently – the volume of related microvoids and bubbles will be lower.

When evaluating this proposed mechanism, a question arises whether it is specific only to Ti-based alloys. Zirconium alloys, for example, are known to form δ-hydride in a delayed manner which causes delayed hydride cracking [47,48]. Extensive research has been carried out on hydrogenation of Zr alloys because of their technological importance [47]; however, no voids or bubbles were reported. In order to examine this, the volume shrinkage due to delayed hydride

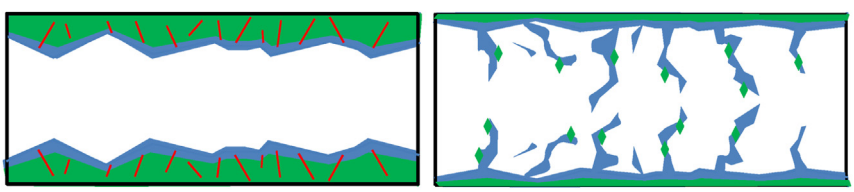

Fig. 5 – Electrochemical hydrogenation of a metal. High hydrogen concentration is indicated by blue color; hydride is indicated by green color. (a) Single-phase metal, and (b) two-phase alloy. (For interpretation of the references to color in this figure legend, the reader is referred to the Web version of this article.)

precipitation in Zr is also shown in Fig. 4 (the data for this calculation is provided in Table 2). Fig. 4 shows that delayed hydride precipitation in Zr is accompanied by less shrinkage than in Ti. Perhaps this is the reason why microvoids/bubbles such as those observed by Navi et al. [10] in Ti–6Al–4V are not observed in Zr-based alloys.

Obviously, the above discussion is not conclusive. For example, the calculation of shrinkage in Ti was done based on data on pure titanium hydrides, while in Ti–6Al–4V we should expect mixed-metal hydrides such as those found in the Ti–Al–H and Ti–V–H systems [49,50]. Also, a combined thermochemical-micromechanical model was not constructed as it is too complicated for our current understanding of the system. However, the comparison between hydrogenation of a single-phase metal and a two-phase alloy did allow us to rule out some possible mechanisms for void formation in Ti–6Al–4V and suggest a mechanism that may explain the phenomena observed experimentally.

Conclusions

From the above analysis of the experimental observations of microvoids in hydrogenated wrought and EBM Ti–6Al–4V alloys and their absence in CP-Ti, the following conclusions can be made:

1) Mechanisms that rely on precipitation of hydrogen gas bubbles from a supersaturated matrix as competing with hydride precipitation can be ruled out because such bubbles (or microvoids) are not observed in electrochemically hydrogenated CP-Ti, in which our calculations concluded they were supposed to be more prevailing than in Ti–6Al–4V.
2) The mechanism that seems to be most likely is based on shrinkage that occurs when the formation of a hydride from supersaturated alloy is delayed and occurs in the bulk of the metal, and not just within a surface layer. The delay in hydride formation could be related to the hydrogenation at low (room) temperature where predominantly fast-diffusing paths through the β phase operate, and so the hydride precipitation may occur far from the surface. In this case, the resulting shrinkage cannot be accommodated by change in the outer dimensions of the sample. Instead, microvoids are formed that can contain hydrogen at pressures that are less than atmospheric. This proposed mechanism does not assume formation of bubbles as a process competing with hydride formation. Instead, the proposed mechanism should lead to microvoids occurring alongside the precipitated hydride, as observed experimentally.
3) The proposed mechanism should result in more hydrogen-related microvoids and bubbles in Ti-based alloys that either contain more α/β interfaces or have lower content of the β phase compared to the α phase.
4) The suggested mechanism can be extended to other hydride-forming alloy systems with exothermic enthalpy of hydrogen solution.

Declaration of competing interest

The authors declare that they have no known competing financial interests or personal relationships that could have appeared to influence the work reported in this paper.

Acknowledgements

This work was supported by grant No. 322/20 from the Pazi Foundation of the Israel Atomic Energy Commission and the Israeli Council of Higher Education. The authors thank Eyal Sabatani for electrochemical hydrogenation; Eliran Hamo for XRD measurements; Zahava Barkay and Yarden Melamed for SEM characterization; David Svetlizky, David Hai David and David Harel for metallographic samples preparation. The authors also thank Prof. Moshe H. Mintz of NRCN and Ben-Gurion University for fruitful discussions.

REFERENCES

[1] Condon JB, Schober T. Hydrogen bubbles in metals. J Nucl Mater 1993;207:1–24.
[2] Völkl J, Alefeld G. Hydrogen diffusion in metals. In: Nowick AS, Burton JJ, editors. Diffusion in solids: recent developments. New York: Academic Press; 1975. Ch. 5.
[3] Zapffe CA, Sims CE. Hydrogen embrittlement, internal stress and defects in steel. Metall Trans AIME 1941;145:225–61.
[4] Tetelman AS, Robertson WD. The mechanism of hydrogen embrittlement observed in iron-silicon single crystals. Trans Met Soc AIME 1962;224:775–83.
[5] Eliaz N, Moshe E, Eliezer S, Eliezer D. Hydrogen effects on the spall strength and fracture characteristics of amorphous Fe-Si-B alloy at very high strain rates. Metall Mater Trans 2000;31:1085–93.
[6] Eliaz N, Eliezer D. Hydrogen effects on an amorphous Fe-Si-B alloy. Metall Mater Trans 2000;31:2517–26.
[7] Eliaz N, Banks-Sills L, Ashkenazi D, Eliasi R. Modeling failure of metallic glasses due to hydrogen embrittlement in the absence of external loads. Acta Mater 2004;52:93–105.
[8] Westlake DG. Equilibrium aspects of hydrogen embrittlement of steels. Trans ASM 1969;62:1000–6.
[9] Birnbaum HK. Mechanisms of hydrogen related fracture of metals. TMS. In: Moody NR, Thompson AW, editors. Proceedings of the fourth international conference on the effect of hydrogen on the behavior of materials. WY: Warrendale; 1990. p. 639–60.
[10] Navi NU, Tenenbaum J, Sabatani E, Kimmel G, Ben David R, Rosen BA, Barkay Z, Ezersky V, Tiferet E, Ganor YI, Eliaz N. Hydrogen effects on electrochemically charged additive manufactured by electron beam melting (EBM) and wrought Ti–6Al–4V alloys. Int J Hydrogen Energy 2020;45:25523–40.
[11] Suwarno S, Maehlen JP, Denys RV, Yartys VA. Effect of oxygen on the mechanism of phase-structural transformations in O-containing titanium hydride. Int J Hydrogen Energy 2019;44:24821–8.
[12] Kong XS, You YW, Fang QF, Liu CS, Chen JL, Luo GN, Pan BC, Wang Z. The role of impurity oxygen in hydrogen bubble nucleation in tungsten. J Nucl Mater 2013;433:357–63.
[13] Tal-Gutelmacher E, Eliezer D. The hydrogen embrittlement of titanium-based alloys. JOM 2005;57:46–9.

[14] Metalnikov P, Eliezer D, Ben-Hamu G, Tal-Gutelmacher E, Gelbstein Y, Munteanu C. Hydrogen embrittlement of electron beam melted Ti–6Al–4V. Int J Mater Res Technol 2020;9:16126–34.
[15] San-Martin A, Manchester FD. The H–Ti (Hydrogen-Titanium) system. Bull Alloy Phase Diagrams 1987;8:30–42.
[16] Gerard DA, Koss DA. The combined effect of stress state and grain size on hydrogen embrittlement of titanium. Scripta Metall 1985;19:1521–4.
[17] Takeuchi Y, Imanishi N, Toyoda K, Uchino T, Iwasaki M. Trapping of hydrogen implanted into titanium. J Appl Phys 1988;64:2959–63.
[18] Sun L, Jin S, Li XC, Zhang Y, Lu GH. Hydrogen behaviors in molybdenum and tungsten and a generic vacancy trapping mechanism for H bubble formation. J Nucl Mater 2013;434:395–401.
[19] Gao J, Cui L, Wan F. Characterization of microstructure in hydrogen ion irradiated vanadium at room temperature and the microstructural evolution during post-irradiation annealing. Mater Char 2016;111:1–7.
[20] Hultgren PJ, Scott TE. Proton-bombardment-induced blistering of vanadium. J Appl Phys 1976;47:4394–400.
[21] Su Z, Wang S, Lu C, Peng Q. Relationship between the behavior of hydrogen and hydrogen bubble nucleation in vanadium. Materials 2020;13:322.
[22] Cullity BD, Stock SR. Elements of X-ray diffraction. 3rd ed., vol. 279. Upper Saddle River, NJ: Prentice Hall; 2001. p. 292. 402.
[23] Kirchheim R, McLellan RB. Electrochemical methods for measuring diffusivities of hydrogen in palladium and palladium alloys. J Electrochem Soc 1980;127:2419–25.
[24] Eliaz N, Eliezer D, Abramov E, Zander D, Köster U. Hydrogen evolution from Zr-based amorphous and quasicrystalline alloys. J Alloys Compd 2000;305:272–81.
[25] Hou J, Kong XS, Wu X, Song J, Liu CS. Predictive model of hydrogen trapping and bubbling in nanovoids in bcc metals. Nat Mater 2019;18:833–9.
[26] Wang K, Kong X, Du J, Li C, Li Z, Wu Z. Thermodynamic description of the Ti–H system. Calphad 2010;34:317–23.
[27] Ukita S, Ohtani H, Hasebe M. Thermodynamic analysis of the Ti-H and Zr-H binary phase diagrams. J Jpn Inst Metals 2007;71:721–9.
[28] Sun P, Fang Z, Koopman M, Paramore J, Ravi Chandran KS, Ren Y, Lu J. An experimental study of the (Ti–6Al–4V)–xH phase diagram using in situ synchrotron XRD and TGA/DSC techniques. Acta Mater 2015;84:29–41.
[29] MacEwen SR, Coleman CE, Ells CE, Faber J. Dilation of h.c.p. zirconium by interstitial deuterium. Acta Metall 1985;33:753–7.
[30] Östberg G, Bergqvist H, Petterson K, Attermo R, Norrgård K, Jansson L-G, Malen K, Papp AE-. Observations of phases and volume changes during precipitation of hydride in zirconium alloys, vol. 499. Stockholm: Atom-Energi; October 1974.
[31] Singh RN, Mukherjee S, Gupta A, Banerjee S. Terminal solid solubility of hydrogen in Zr-alloy pressure tube materials. J Alloys Compd 2005;389:102–12.
[32] Slattery GF. The effect of hydride on the thermal expansivity of zirconium alloys. J Less Common Met 1966;11:89–98.
[33] de Menibus AH, Guilbert T, Auzoux Q, Toffolon C, Brachet JC, Bechade JL. Hydrogen contribution to the thermal expansion of hydrided Zircaloy-4 cladding tubes. J Nucl Mater 2013;440:169–77.
[34] Zanellato O, Preuss M, Buffiere JY, Ribeiro F, Steuwer A, Desquines J, Andrieux J, Krebs B. Synchrotron diffraction study of dissolution and precipitation kinetics of hydrides in Zircaloy-4. J Nucl Mater 2012;420:537–47.
[35] Millenbach P, Givon M. The electrochemical formation of titanium hydride. J Less Common Met 1982;87:179–84.
[36] Yan JY, Olson GB. Molar volumes of bcc, hcp, and orthorhombic Ti-base solid solutions at room temperature. Calphad 2016;52:152–8.
[37] Adler PN, Schulte RL. Stress-induced hydrogen concentration in titanium. Grumman Aerospace Corp; March 1981. https://apps.dtic.mil/sti/citations/ADA098100. Report RE-624, New York.
[38] Lynch JF, Tanaka J. Thermodynamics of the solid solution of hydrogen in β-titanium alloys: β-TiMo and β-TiRe. Acta Metall 1981;29:537–45.
[39] Waisman JL, Sines G, Robinson LB. Diffusion of hydrogen in titanium alloys due to composition, temperature, and stress gradients. Metall Trans 1973;4:291–302.
[40] Zuzek E, Abriata JP, San-Martin A, Manchester FD. The H-Zr (hydrogen-zirconium) system. Bull Alloy Phase Diagrams 1990;11:385–95.
[41] Lu XG, Selleby M, Sundman B. Assessments of molar volume and thermal expansion for selected bcc, fcc and hcp metallic elements. Calphad 2005;29:68–9.
[42] Eadie RL, Tashiro K, Harrington D, Léger M. The determination of the partial molar volume of hydrogen in zirconium in a simple stress gradient using comparative microcalorimetry. Scripta Metall Mater 1992;26:231–6.
[43] Fukai Y. The metal-hydrogen system. New York: Springer-Verlag; 1993. p. 22.
[44] Luo L, Su Y, Guo J, Fu H. Formation of titanium hydride in Ti–6Al–4V. J Alloys Compd 2006;425:140–4.
[45] Liu HJ, Zhou L, Liu P, Liu QW. Microstructural evolution and hydride precipitation mechanism in hydrogenated Ti–6Al–4V alloy. Int J Hydrogen Energy 2009;34:9596–602.
[46] Kim J, Tasan CC. Microstructural and micro-mechanical characterization during hydrogen charging: an in situ scanning electron microscopy study. Int J Hydrogen Energy 2019;44:6333–43.
[47] Motta AT, Capolungo L, Chen LQ, Cinbiz MN, Daymond MR, Koss DA, Lacroix E, Pastore G, Simon PCA, Tonks MR, Wirth BD, Zikry MA. Hydrogen in zirconium alloys: a review. J Nucl Mater 2019;518:440–60.
[48] Zhao C, Song X, Yang Y, Zhang B. Hydrogen absorption cracking of zirconium alloy in the application of nuclear industry. Int J Hydrogen Energy 2013;38:10903–11.
[49] Rudman PS, Reilly JJ, Wiswall RH. The formation of metastable hydrides $Ti_{0.75}Al_{0.25}H_x$ with $x < 1.5$. J Less Common Met 1978;58:231–40.
[50] Hagi T, Sato Y, Yasuda M, Tanaka K. Structure and phase diagram of Ti-V-H system at room temperature. Trans Jpn Inst Metals 1987;28:198–204.